Integrating boron nitride and hydroxylated graphene in phase-change films for flexible electronics cooling

Xuehong Wu [a,c], Mengyao Liu [a], Yanbo Pan [b], Yong Liu [a,c], Cai Lv [a,c], Zhijuan Chang [b,d] and Yanping Du[e, *]

a School of Energy and Power Engineering, Zhengzhou University of Light Industry, Zhengzhou, Henan 450000, China

b School of Food and Bioengineering, Zhengzhou University of Light Industry, Zhengzhou, Henan 450000, China

c International Joint Laboratory for Efficient Energy Conversion and Utilization of Henan Province, Zhengzhou, Henan 450000, China

d Key Laboratory of Cold Chain Food Processing and Safety Control of the Ministry of Education, Zhengzhou, Henan 450000, China

e School of Engineering, Lancaster University, Lancaster LA14YW, UK

** Corresponding author: y.du17@lancaster.ac.uk*

Abstract: With the rapid development of flexible electronic technologies, there is a growing demand for high-performance, flexible thermal interface materials (TIMs) capable of efficiently dissipating heat while conforming to complex device geometries. Phase-change films (PCFs), owing to their inherent latent heat storage capabilities and favorable processability, have emerged as promising candidates for such applications. However, integrating high thermal conductivity with effective phase-change functionality and mechanical flexibility remains a major technical challenge. In this study, a series of novel phase-change films (PCFs) were successfully fabricated using a solvent evaporation method. Polylactic acid (PLA) served as the support material, polyethylene glycol (PEG) acted as the phase-change medium, and highly thermally conductive particles including boron nitride (BN) and hydroxylated graphene (OH-GN) were employed as thermal conductive fillers to establish efficient heat conduction pathways. The experimental results indicate that the composite PCFs exhibit excellent thermal reliability and functional performance in diverse conditions. The newly fabricated PCFs demonstrate strong leakage resistance at 80 °C, high phase-change enthalpy (>97.95 J/g), and enhanced thermal stability, while maintaining good mechanical flexibility. The thermal conductivity of the PCFs was significantly improved with

the addition of conductive fillers. Specifically, the incorporation of 20 wt% BN increased the thermal conductivity to 0.40 W/(m·K), marking a 222.22% enhancement over the baseline PLA/PEG film. Notably, the composite PCFs containing 9 wt% OH-GN achieved the highest thermal conductivity of 0.86 W/(m·K), corresponding to a 477.78% increase. Furthermore, OH-GN significantly enhanced the photothermal conversion performance of the PCFs due to its strong light absorption. The PCF-11 (with 9 wt% OH-GN) exhibited a photothermal conversion efficiency of 91.7%. Under a controlled environment at 45 °C, the temperature of a pure PLA film rapidly rose to 44 °C, whereas the PCF-11 exhibited a slower and more stable temperature increase, indicating effective thermal buffering. These results confirm the substantial potential of the composite PCFs in next-generation thermal management applications for flexible and wearable electronic devices.

Keywords: Phase change films (PCFs); Thermal management; Mechanical flexibility; Leakage resistance; Thermal stability

Nomenclature

ΔH	Enthalpy (J/g)
T	Temperature (°C)
t	Time (s)
m	Gram(g)
A	Surface area (cm2)
Δt	Time (s)
P	Power (mW/cm^2).
Subscripts	
m	Melting
c	Crystallization
Greek symbols	
λ	Photothermal conversion efficiency
Abbreviations	
TIMs	Thermal interface materials
PCFs	Phase change films
PLA	Polylactic acid
PEG	Polyethylene glycol
BN	Boron nitride
OH-GN	Hydroxylated graphene
PCMs	Phase-change materials

CPCM	Composite phase change material
PVA	Polyvinyl alcohol
PVDF	Polyvinylidene fluoride
PU	Polyurethane
PE	Polyethylene

Abbreviations

PCMC	Phase-change microcapsules
PGAMF	Polyethylene glycol/graphene/carbon nanotube-PCMC composite film
PW	Paraffin
PEG/WF	Polyethylene glycol/wood flour
3D	Three-dimensional
DCM	Dichloromethane
FTIR	Fourier Transform Infrared Spectrometer
XRD	X-ray diffraction analyzer

1. Introduction

The high integration of electronic devices is normally accompanied by increasing power density and limited heat dissipation capacity, resulting in difficulty in effectively dissipating the heat accumulated during operation[1, 2]. Excessive heat accumulation can lead to decreasing performance of electronic components and even damage the devices due to the thermal runaway. The existing active cooling technologies consume extra electricity to drive the working fluid (i.e. water), which significantly increases the cost and may lead to short circuit of electronics due to leakage. While for the conventional passive cooling technologies such as structured fins (with fans), and heat pipes, the cooling effectiveness is good but is significantly restrained by the volume and shape of the electronics considering the thermal resistance caused by rough surfaces. Phase-change materials (PCMs) can store and release thermal energy through their phase transition process attributed to their high energy density, minimal volume change, and relatively constant phase-change temperature. Therefore, it is essential to develop a PCM based thermal management system that can be flexibly applied for electronics cooling. Solid-liquid organic PCMs have demonstrated significant potential for applications in thermal management [3, 4]. PEG has garnered widespread interest and research due to its excellent latent heat of phase change, ex-

ceptional chemical stability, low supercooling, cost-effectiveness, and non-corrosive properties[5-7]. Cheng[8] synthesized shape-stable polyethylene glycol/titanium dioxide composite phase-change materials (CPCM) using titanium butoxide as a precursor through a simple sol-gel method. The fabricated CPCM exhibited melting and crystallization enthalpies of 128.3 J/g and 113.1 J/g, respectively, with an encapsulation efficiency of 74.14%. Lu et al[9] first utilized MXene as a support framework and PEG as the phase-change material to fabricate a composite, PEG@MXene, with an excellent thermal conductivity via a simple vacuum impregnation method. The material demonstrated a melting latent heat of 131.2 J/g and a crystallization latent heat of 129.5 J/g, with a relative enthalpy efficiency of 80.3%. These results highlight the significant potential of the PEG-based material for thermal energy storage applications.

However, the inherent issues of leakage, rigidity, and low thermal conductivity in organic phase-change materials[10, 11] present significant challenges in their thermal management applications. Phase-change materials are prone to leak during the melting process[12, 13]，which necessitates their encapsulation using suitable carriers. Currently, the primary encapsulation methods include polymer encapsulation[14], metal encapsulation[15], and ceramic encapsulation[16]. Rigid materials are unable to conform perfectly to electronic devices, leading to a reduced thermal management efficiency[14, 17]. Therefore, it is crucial to develop flexible phase-change materials with a high encapsulation efficiency. While metals lack the necessary flexibility to serve as encapsulation substrates for phase-change materials, ceramics, though offering excellent hardness, thermal conductivity, and corrosion resistance, are limited by their brittleness in applications that require flexibility. Polymer matrices, by imparting toughness and excellent processability to materials, have widespread applications in fields such as electronic packaging and protective coatings. From the perspective of flexibility, polymers are clearly superior to existing attempted materials such as ceramics. By dispersing small-molecule phase-change materials into a macromolecular polymer matrix, shape-stable flexible composite phase-change materials can be syn-

thesized. In this process, the polymer matrix serves as a support, preventing the leakage of liquid PCM.

Polymers commonly used as support materials in fabrication composite phase change materials. Examples include polyvinyl alcohol (PVA)[18, 19], polyvinylidene fluoride (PVDF)[20, 21], polyurethane (PU)[22, 23] and polyethylene (PE)[24, 25]. Zhao et al[26] synthesized amine-modified multi-walled carbon nanotube phase-change microcapsules (PCMC) and prepared a flexible polyethylene glycol/graphene/carbon nanotube-PCMC composite film (PGAMF) with a three-dimensional sandwich structure using a simple casting method. The prepared PGAMF film exhibited a phase change enthalpy of 45.5 J/g. The sandwich structure, reinforced by the binding effect of PVA, effectively anchors the carbon nanotube-PCMC microcapsules within the PGAMF film, preventing detachment or sliding. This design endows the PGAMF composite film with an excellent flexibility. Zhang et al[27] developed flexible composite phase-change film with a high thermal conductivity by using a porous polyvinylidene fluoride-boron nitride film as the substrate and paraffin (PW) as the phase-change material. The flexible composite phase-change film exhibited an excellent melting enthalpy of 105.63 J/g and a thermal conductivity that was 200% higher than that of pure PW. Additionally, the film maintained outstanding flexibility at room temperatures and demonstrated an excellent cycling stability, further improving its suitability for thermal management of electronic devices. Aftab et al[28] prepared a polyurethane-impregnated carbon nanotube composite material. In this structure, PEG was confined within the PU matrix while also infiltrated the pores of the carbon nanotube sponge, resulting in shape-stable and flexible phase-change composite materials. The results showed that the CPCM had an energy storage density of 132 J/g. Tang et al[29] prepared a stearyl alcohol/high-density polyethylene/ethylene glycol composite phase-change material using high-density polyethylene as the substrate for thermal energy storage, with a latent heat of up to 200 J/g. Currently, although various flexible phase-change materials employ the aforementioned polymers as supporting matrices, these substrates are typically

non-biodegradable, posing challenges to environmentally sustainable and low-carbon development goals. Furthermore, their relatively high production costs and intricate fabrication processes hinder large-scale implementation and limit their practical applications in cost-sensitive or eco-conscious contexts.

In contrast, polylactic acid (PLA), as an emerging polymer, has attracted increasing attention due to its excellent biodegradability, good compatibility and low cost. Existing methods for encapsulating phase-change materials with PLA primarily include melt blending, capsule encapsulation, porous adsorption, and spiral extrusion granulation. Geng et al[30] prepared a shape-stable and processable phase-change composite material by melt-blending PLA and PEG at 180 °C, with the PEG mass fraction reaching up to 90%. Zhang et al[31] used polylactic acid as the shell material and n-hexadecane as the phase-change material and successfully prepared a series of n-hexadecane/polylactic acid phase-change microcapsules with different compositions. Experimental results indicated that when a 5% PLA/chloroform solution was used as the matrix for encapsulating n-hexadecane, the encapsulation efficiency could reach approximately 100%, and the phase-change enthalpy was 97 J/g. Yang et al[32] first prepared aerogels with high porosity (>90%) and utilized their porous structure to encapsulate paraffin, successfully obtaining shape-stable bio-based phase-change materials. The results demonstrated that the composite phase-change material retained a high latent heat of 169.5 J/g and exhibited excellent leakage resistance. Sheng et al[33] adopted a polyethylene glycol/wood flour (PEG/WF) composite as the latent heat medium, with polylactic acid as the matrix, and used a twin-screw eccentric rotor and pelletizer to prepare PEG/WF composites. The study showed that, due to capillary forces, PEG was easily encapsulated by the wood flour. After incorporating PLA, the PEG/WF/PLA ternary composite still exhibited a high latent heat of 87.2 J/g. Because PEG and PLA exhibited a good compatibility, they can be blended into a solution. Currently, most studies on PEG/PLA blend materials focus on enhancing the flexibility of PLA by incorporating PEG. Kumar et al[34] successfully prepared 3D-printed PLA/PEG samples using fused deposition modeling technology. By incorporating 5%

PEG into the PLA matrix, a PLA/PEG blend was synthesized. The results showed that the mechanical properties of the blend were significantly improved compared to pure PLA. Wang et al[35] investigated the use of PEG as a plasticizer to enhance the toughness of PLA. The experimental results indicated that the incorporation of PEG effectively plasticizes PLA. Although various methods have been employed to incorporate phase change materials into PLA matrices, most research has predominantly emphasized improving the mechanical flexibility of PLA by introducing PEG with different molecular weights. However, limited attention has been given to systematically investigating the phase change behavior and thermal storage performance of PLA-based composites containing PEG of varying molecular weights, leaving a gap in understanding the structure and property relationships critical for thermal energy storage applications.

Similar to organic phase change materials, most polymer matrices inherently possess low thermal conductivity, which significantly limits the overall thermal performance of composites PCM/polymer-based energy storage system. To overcome this limitation, the incorporation of thermally conductive fillers is essential for achieving a significantly efficient thermal management system for electronics. Currently, the primary method for enhancing the thermal conductivity of phase change materials is the incorporation of high thermal conductivity fillers [36, 37], such as incorporating carbon nanotubes [38, 39], graphene [40, 41], boron nitride [42, 43], and MXene [9, 44] into PEG. However, carbon nanotubes suffer from poor dispersion in polymer matrices, leading to aggregation, which can hinder improvements in both thermal conductivity and mechanical properties. Although MXene is a promising emerging material, its long-term performance and processing technologies are not yet as advanced as those of graphene and boron nitride. Mao et al[45] developed a composite phase change material through modified graphene aerogel that demonstrates exceptional thermal properties: the thermal conductivity was enhanced by 213.8% compared to pure PEG, with a phase change enthalpy of 163.07 J/g. Remarkably, the material retained 90.02% of its enthalpy after 500 thermal cycles. These key metrics

conclusively demonstrate graphene's outstanding performance in both thermal conductivity enhancement and thermal energy storage stability. Zhou et al[46] developed a BN/PEG composite phase change material demonstrating outstanding performance metrics: a thermal conductivity of up to 0.89 W/(m·K) and a phase change enthalpy of 183.07 J/g (retaining 97% of pure PEG's heat storage capacity). The experimental results conclusively demonstrated that both graphene and boron nitride serve as highly effective functional fillers for significantly enhancing the thermal conductivity of PEG-based phase change materials.

Building on the above context, this study aims to overcome the key performance limitations of conventional phase change materials (PCMs) in electronic thermal management by developing multifunctional and flexible composite phase change films (PCFs). Through a synergistic approach integrating material selection and structural design, polyethylene glycol (PEG) was employed as the phase change energy storage medium, while polylactic acid (PLA) served as a flexible support matrix. To establish efficient thermal conduction pathways, thermally conductive fillers including boron nitride (BN) and hydroxylated graphene (OH-GN) were incorporated into the composite system. A solvent evaporation-assisted casting process was utilized to fabricate the PLA/PEG/BN and PLA/PEG/OH-GN composite films.

In experiments, the resulting composite phase change films (PCFs) exhibit notably enhanced overall performance. These include high phase change enthalpy and substantial improvements in thermal conductivity, mechanical flexibility and conformability to various surface geometries. Experimental results show that the films can adhere closely to electronic component surfaces, effectively regulating operating temperatures while maintaining stable performance across multiple thermal cycles. This synergistic design strategy addresses the inherent shortcomings of traditional PCMs in electronic thermal regulation, offering strong application potential in high-power electronic devices and related fields.

2. The preparation and characterization of composite PCFs

2.1 Fabrication of composite PCFs

The materials used in this study include polyethylene glycol and polylactic acid, with their specific parameters provided in Table 1. The instruments and equipment used for material preparation and characterization, along with their model numbers and manufacturers, are listed in Table 2.

Table 1. Experimental materials.

Experimental Materials	Specific Information	Origin and Manufacturer
Polyethylene glycol	PEG:1000，37.58 ℃	Shanghai Maclean Co., Ltd.
Polylactic acid	2003D	Nature Works, Inc.
Dichloromethane (DCM)	CH_2Cl_2，Purity>99.9%	Tianjin Fuyu Fine Chemical Co., Ltd.
Boron Nitride	1um，Purity 98.5%	Shanghai Maclean Co., Ltd.
Hydroxylated graphene	Single layer	Guoheng Qihang Technology Co., Ltd.

Table 2. Experimental instrument.

Instrument Name	Instrument model and test accuracy	Manufacturer
Electronic balance	ME2004(0.1mg)	Mettler-Toledo Instruments Ltd.
Differential Scanning Calorimeter	DSC241(error 1%；±0.1 ℃)	Germany Netzsch Technology Co., Ltd.
Thermal conductivity instrument	LFA467(error 1%；±0.1 ℃)	Germany Netzsch Technology Co., Ltd.
Infrared thermal imager	FLIR T640(±2 ℃)	Beijing Huayi Tongtai Technology Co., Ltd.
X-ray diffraction analyzer	D8 ADVANCE	Bruker Scientific
Fourier Transform Infrared Spectrometer	FTIR-8400b	Shimadzu Co., Ltd.
Solar Simulator	7IS1003A	Beijing Saifan Optoelectronics Instrument Co., Ltd.
Electric blast drying oven	DHG-9070(±0.5 ℃)	Shanghai Yiheng Scientific Instrument Co., Ltd.

Universal tensile testing machine	BT1-FB005TN.14	Zwick Company
High and low temperature test chamber	WGDW-100（±2 ℃）	Wenzhou Weidu Electronics Co., Ltd.

The preparation process of the flexible phase change film is illustrated in Figure 1(a). First, high thermal conductivity particles with varying mass fractions were added to 50 mL of dichloromethane and dispersed thoroughly using an ultrasonic oscillator. Then, 3 g of polylactic acid was added to the solution and stirred with a magnetic stirrer at room temperature for 1 hour until the PLA was completely dissolved. Next, PEG was incorporated into the solution and stirred for an additional 0.5 hours at room temperature to form a uniform blending solution. Finally, the homogeneous solution was cast onto a glass plate using the casting method. After air-drying at room temperature for 12 hours, the film was further dried in an oven for 6 hours to ensure complete evaporation of the dichloromethane, resulting in the phase change film. The encapsulation mechanism of the phase change film is illustrated in Figure 1(b). PEG and thermal conductive particles were encapsulated within the mesh structure of PLA, effectively restricting the flow of liquid PEG. The appearance of the PLA, PLA/PEG/BN, and PLA/PEG/OH-GN films is shown in Figures 1(c-e). The PLA film appears transparent, while the addition of BN and PEG gradually turns the film milky white. Upon the inclusion of OH-GN, the film gradually becomes black. The detailed composition and names of the PLA/PEG/(BN/OH-GN) flexible films are provided in Table 3.

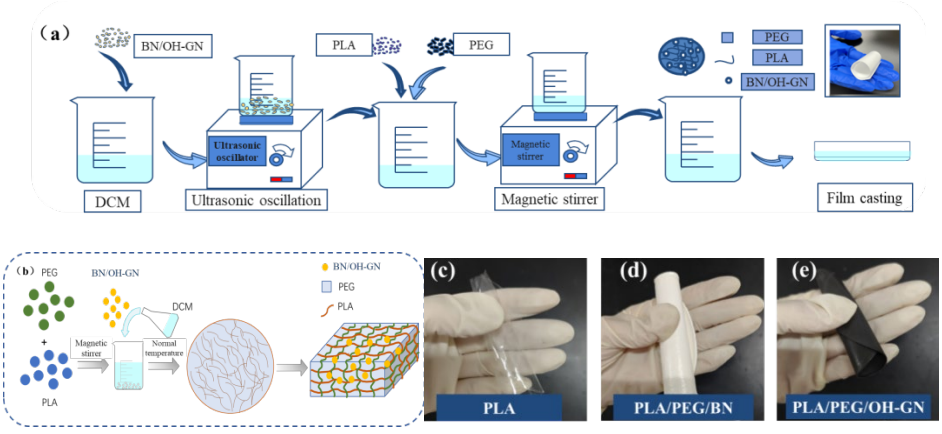

Figure 1 (a) Preparation flow chart of high thermal conductivity phase change film; (b)

Packaging principle diagram of high thermal conductivity phase change film; (c-e) appearance of PLA, PLA/PEG/BN, and PLA/PEG/OH-GN films.

Table 3. Composition of PLA/PEG/(BN/OH-GN) Phase Change Films.

Sample	PLA(g)	PEG(g)	BN(g)	OH-GN(g)
PEG1000	-	3	-	-
PLA/PEG	3	7.5	-	-
PCF-1	3	7.5	0.325	-
PCF-2	3	7.5	0.55	-
PCF-3	3	7.5	0.79	-
PCF-4	3	7.5	1.038	-
PCF-5	3	7.5	1.85	-
PCF-6	3	7.5	2.625	-
PCF-7	3	7.5	-	0.105
PCF-8	3	7.5	-	0.325
PCF-9	3	7.5	-	0.55
PCF-10	3	7.5	-	0.79
PCF-11	3	7.5	-	1.038

The characterization of thin films includes thermal property analysis, chemical structure analysis, thermal conductivity analysis, mechanical behavior analysis, and thermal management performance analysis. The specific details are as follows:

(1) Thermal performance analysis: The phase transition temperature and enthalpy of the phase change material were measured using a differential scanning calorimeter (DSC241, NETZSCH Scientific Instruments Trading Co., Ltd., accuracy: 1%; ±0.1°C) under a nitrogen atmosphere at a heating/cooling rate of 10 °C/min.

(2) Chemical structure analysis: The FTIR spectra of the thin-film samples were recorded using a Japanese FTIR-8400b Fourier transform infrared spectrometer, with a scanning range of 400–4000 cm^{-1} and a resolution of 2 cm^{-1}. X-ray diffraction analysis was performed on the samples within a 2θ range of 5°–90°.

(3) Thermal conductivity analysis: The thermal diffusivity of the thin-film samples was measured using a German LFA467 HyperFlash® thermal conductivity analyzer at room temperature, while the specific heat capacity was determined by DSC241 differential scanning calorimetry.

(4) Mechanical behavior analysis: The phase-change film was prepared into strip-shaped samples measuring 50×10×0.5 mm^3. Tensile tests were conducted at

room temperature using a universal testing machine with a crosshead speed of 20 mm/min, in accordance with the international standard GB13022-91 "Test Method for Tensile Properties of Plastic Films."

(5) Thermal management performance analysis: To evaluate the thermal regulation characteristics of the thin film, an electronic heating platform was employed to simulate the operating conditions of electronic devices, with the test film sample placed at the center of the heating zone. An Agilent data acquisition unit (KEYSIGHT-34972A, ±0.2 °C) was used to monitor the sample temperature for thermal management characterization, while an infrared thermal imager (FLIR T640, ±2 °C) simultaneously recorded real-time surface temperature distribution of the sample.

2.2 Preparation and Characterization Methods of Composite Phase Change Films

FTIR spectroscopy was used to examine the T chemical composition of the flexible phase change films. The FTIR spectra of PLA, PEG, DCM, and PLA/PEG are presented in Figure 2(a). For PLA, the characteristic peak at 1745 cm^{-1} is attributed to the C=O stretching vibration, which corresponds to the ester group in PLA molecules. The peaks at 1082 cm^{-1} and 1181 cm^{-1} are associated with the C-O-C stretching vibrations, while the peak between 1450 cm^{-1} and 1380 cm^{-1} is attributed to the stretching vibration of the $–CH_3$ group. In the FTIR spectrum of PEG, the characteristic peaks at 2869 cm^{-1} and 1455 cm^{-1} are attributed to the stretching and bending vibrations of the $–CH_2$- group, respectively. The peak in the range of 3500-3400 cm^{-1} corresponds to the stretching vibration of the -OH group. In the FTIR spectrum of the PLA/PEG composite, the characteristic peaks of both PLA and PEG are observed, while no peaks corresponding to DCM are detected. This indicates that the structures of PLA and PEG remain unchanged, demonstrating that PLA can effectively encapsulate PEG.

The FTIR spectra of PLA/PEG, BN, and PLA/PEG/BN are shown in Figure 2(b). The characteristic peak at 2877 cm^{-1} in the PLA/PEG spectrum corresponds to the C–

H stretching vibration in PEG molecules, while in the PLA/PEG/BN film, the corresponding peak shifts to 2881 cm^{-1}. The peak at 1750 cm^{-1} is typically associated with the ester group (C=O), representing the carbonyl stretching vibration in PLA, and this peak shifts to 1751 cm^{-1} in the PLA/PEG/BN film. The characteristic peak at 1093 cm^{-1} corresponds to the C–O stretching vibration, which shifts to 1097 cm^{-1} in the PLA/PEG/BN film. The peak at 948 cm^{-1} is associated with the C–H bending vibration in PLA, particularly related to the vibration of certain methylene groups (–CH_2–), and shifts to 949 cm^{-1} in the PLA/PEG/BN film. The characteristic peaks at 827 cm^{-1} and 1350 cm^{-1} for BN are attributed to B–N bending vibrations, which correspond to the peaks at 830 cm^{-1} and 1348 cm^{-1} in the PLA/PEG/BN film. The corresponding FTIR spectra for PLA/PEG, OH-GN, and PLA/PEG/OH-GN are shown in Figure 2(c). The characteristic peak at 2885 cm^{-1} for OH-GN is typically attributed to the C–H stretching vibrations, especially related to the C–H groups present on the surface of hydroxylated graphene oxide. This peak represents the stretching vibration of the C–H bonds in OH-GN and corresponds to the 2886 cm^{-1} peak in the PLA/PEG/OH-GN film. The characteristic peak at 1102 cm^{-1} is generally associated with C–O stretching vibrations, which is related to the hydroxyl groups in OH-GN. This peak is also present in the PLA/PEG/OH-GN film, with no additional new peaks. Therefore, it can be concluded that the encapsulation of PLA/PEG with BN or OH-GN is a physical process.

To investigate the crystallization behavior of the materials and PCF, X-ray diffraction (XRD) analysis was performed on the samples in the 2θ range of 5° to 90°. The results are shown in Figures 2(d-f). PLA exhibits a weak and broad diffraction peak around 17°, indicating poor crystallization, while PEG shows two sharp and intense diffraction peaks at 19.3° and 23.4°, indicating better crystallization capability compared to PLA. The XRD pattern of the PEG/PLA phase change films shows absorption peaks similar to those of PEG, but with a reduced intensity of the diffraction peaks. This is due to the PLA chains restricting the crystallization of PEG, which results in a smaller crystallized region of PEG in the presence of PLA. Due to the phys-

ical mixing of PLA and PEG, PLA effectively encapsulates PEG. With the addition of BN, the XRD pattern of PEG/PLA/BN shows high-intensity diffraction peaks from PEG/PLA and low-intensity peaks from BN, indicating that the crystallized region of PEG/PLA/BN increases with the introduction of BN. In contrast, the XRD pattern of PEG/PLA/OH-GN shows low-intensity diffraction peaks from both PEG/PLA and OH-GN, suggesting a reduction in the crystallized region of PEG/PLA/OH-GN with the incorporation of PEG/PLA and OH-GN. No new diffraction peaks are observed, confirming that PLA/PEG with BN or OH-GN is synthesized through a physical process.

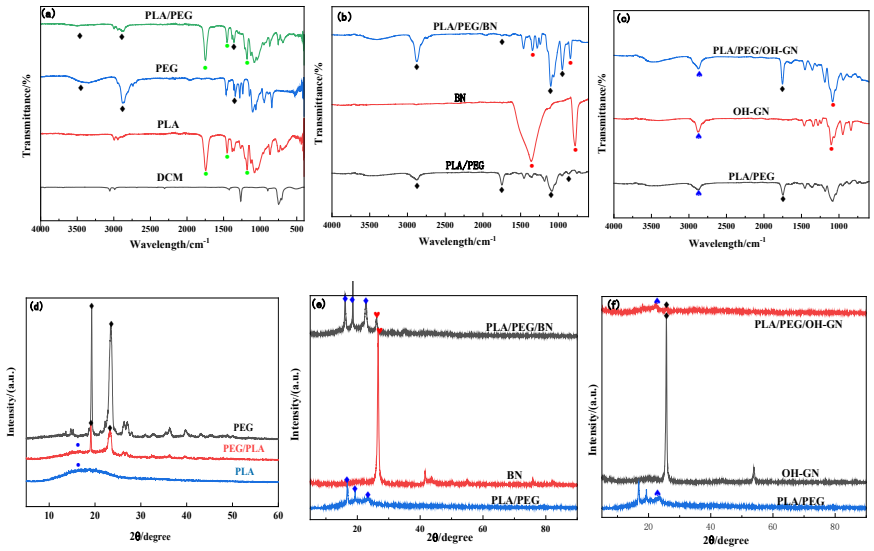

Figure 2 (a) FT-IR absorption spectra of PLA, PEG, PEG/PLA and DCM; (b) FT-IR absorption spectra of PEG/PLA, BN and PLA/PEG/BN; (c) FT-IR absorption spectra of PEG/PLA, OH-GN and PLA/PEG/OH-GN; (d) XRD curves of PLA, PEG and PEG/PLA; (e) XRD curves of PEG/PLA, BN and PLA/PEG/BN; (f) XRD curves of PEG/PLA, OH-GN and PLA/PEG/OH-GN.

3. The structural superiority of the composite PCFs

3.1 Mechanical properties and deformation analysis

Mechanical properties are essential for the practical application of thin films. To assess the mechanical performance of the phase-change films, a series of uniaxial tensile tests were conducted. Figures 3(a-c) presents the stress-strain curves and elastic moduli of films with varying amounts of BN and OH-GN. The elongation of pure

PLA film is approximately 2%, with a tensile strength of 14.5 MPa. After the addition of PEG, the elongation of the PLA/PEG film significantly increases to 65%, while its tensile strength decreases to approximately 3 MPa. PEG acts as both a phase change material and a plasticizer, enhancing the mobility of PLA chains. As the BN content increases from 3% to 20%, the elongation of the PCF decreases from 53% to 18%, and the elastic modulus decreases from 62.42 MPa to 49.5 MPa. When the OH-GN content increases from 1% to 9%, the elongation of the PCF decreases from 75.8% to 10.2%, and the elastic modulus decreases from 59.18 MPa to 19.07 MPa. Since the Young's modulus presented in Fig. 3c is derived from the raw data and corresponding fitting curves in Figs. 3a and 3b, the associated uncertainty has been inherently incorporated through the measurement and analysis process. From the above analysis, it can be concluded that with the increase in BN or OH-GN content, the elongation at break of the films gradually decreases, indicating a reduction in toughness and a higher tendency for fracture during stretching. This is possibly due to the presence of BN and OH-GN, which reduces the ductility of materials. Moreover, the decrease in elastic modulus suggests a reduction in the rigidity of materials, resulting in a gradual loss of flexibility. However, compared to pure PLA films, these composite films still retain a good flexibility. Additionally, the phase-change films can be easily shaped into various complex forms and folded without compromising their integrity. The bending and cutting performance of the films at room temperatures are shown in Figures 3(d-g). As demonstrated, the films exhibit an excellent bending flexibility, deformability, and exceptional cutability, which enhances their potential for efficient thermal management in compact electronic devices.

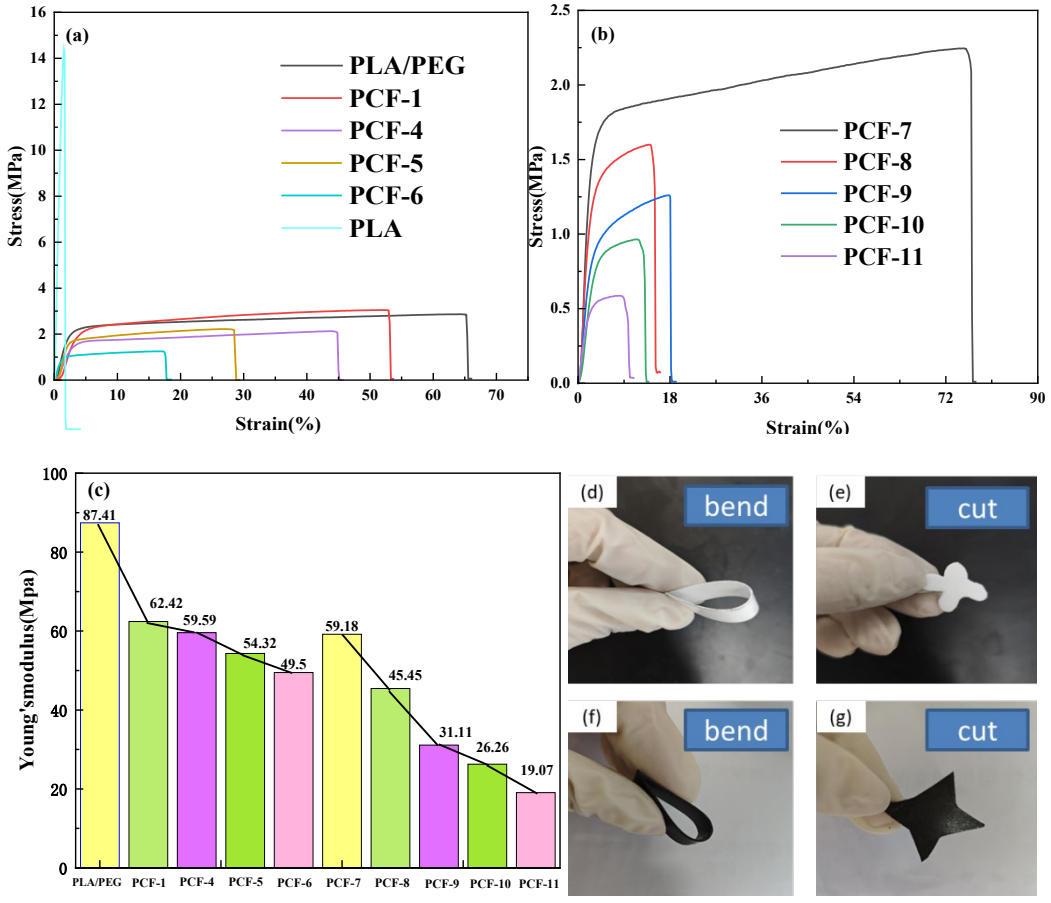

Figure 3 (a) Stress-strain curves of PLA, PEG/PLA and PEG/PLA/BN films; (b) Stress-strain curve of PEG/PLA/OH-GN film; (c) the elastic modulus of the film; (d) The bending diagram of PLA/PEG/BN film; (e) Shear diagram of PLA/PEG/BN film; (f) The bending diagram of PLA/PEG/OH-GN film; (g) Shear diagram of PLA/PEG/OH-GN film.

3.2 Leakage prevention analysis

Shape stability is a critical requirement for the practical application of phase change materials, as it significantly broadens their usability. This study investigated the leakage performance of PEG, PLA/PEG/BN, and PLA/PEG/OH-GN at 25 °C and 80 °C, respectively. The results are illustrated in Figure 4. During the heating process from 25 °C to 80 °C, the PEG material absorbs phase change latent heat and undergoes a solid-to-liquid phase transition.

In the experimental study, the filter paper method was employed to visually and reliably demonstrate the leak prevention characteristics. As can be seen from Figure 4,

throughout the heating process, the surface of the filter paper remains clean and there are no visible traces of polyethylene glycol leakage. This indicates that due to the encapsulation of polylactic acid and the unique spatial confinement effect of its three-dimensional network structure, the molten polyethylene glycol does not breach the polylactic acid matrix. Therefore, the phase transition process of polyethylene glycol is effectively confined within this porous framework. It is worth noting that when the polyethylene glycol completely melted into a liquid and the temperature reaches 80°C or higher, no leakage phenomenon was observed on the surface of the PLA/PEG/Boron Nitride and PLA/PEG/Hydroxy Graphene Nanotube composite phase change films. In addition, a quantitative analysis of PEG leakage was conducted to evaluate the shape stability of the composite fibers. From the leakage loss rate presented in Figure 4 (g), it can be seen that although the PLA/PEG/BN sample has a slightly higher leakage amount than the PLA/PEG/OH-GN sample after heating at 80°C for 2 hours, the leakage rates of both samples remain within 5%. This indicates that due to the addition of polylactic acid, the composite polylactic acid/PEG/Boron Nitride (i.e., polyethylene glycol/(Boron Nitride/Hydroxy Graphene Nanotube)) phase change fibers have excellent encapsulation and shape stability over a wide temperature range.

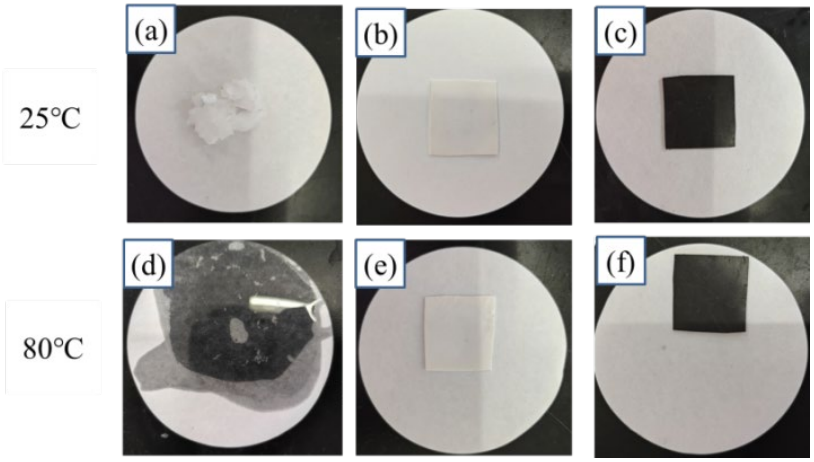

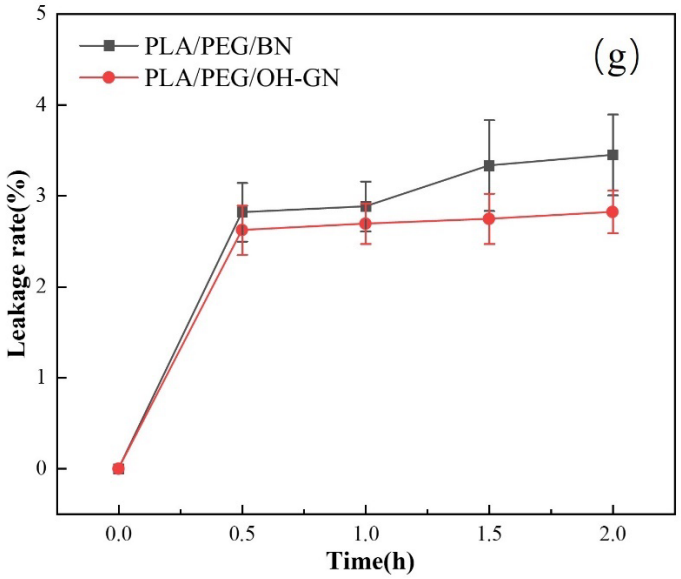

Figure 4. Leakage prevention of PEG, PLA/PEG/BN and PLA/PEG/OH-GN films at 25 and 80 ℃.

4 Thermal performance of the composite PCFs

4.1 Phase change behaviors of composite PCFs

To evaluate the heat storage performance of the composite phase change films, DSC tests were conducted on PEG and phase change films with different compositions. The DSC curves of the various materials in the temperature ranging from -20 °C to 80 °C are presented in Figures 5(a-b) and 6(a-b). During the heating process, all materials except PCF4 show a melting peak for PEG around 38 °C, indicating the solid-liquid phase transition of PEG. Since the melting point of PLA is much higher than 80 °C, no characteristic peak of PLA is observed within this temperature range. The melting temperature (T_m) of the PLA/PEG composite is 39 °C, with a melting enthalpy (ΔH_m) of 124.7 J/g. The unique phase transition behavior observed in PCF-4 samples with 1.038 wt% boron nitride addition originates from a critical concentration effect, which has been validated by our repeated experiments and subsequent investigations. With a BN concentration below this threshold, the nanosheets maintain a good dispersion but fail to establish an effective thermal network. While with a concentration of BN over the threshold, nanosheet agglomeration occurs predominantly. The specific 1.038 wt% formulation enables BN fillers to form an optimal

three-dimensional thermal conductive network, which significantly modifies the crystallization behavior of the PEG matrix. This particular concentration not only optimizes the heat transfer pathways but also regulates the crystallization process through distinctive interfacial interactions, which explains for the characteristic phenomenon of reduced melting enthalpy coupled with left-shifting crystallization temperature. Although thermal percolation is not as widely accepted as electrical percolation in composite materials, recent studies have increasingly reported similar threshold-like behaviors in thermally conductive nanocomposites. In this context, the observed transition of composite PCF-4 at 1.038 wt% may be reasonably interpreted within the framework of thermal percolation. This concentration-dependent transition in phase change properties aligns well with the typical percolation threshold effect observed in nanocomposite materials.

The crystallization temperature (T_C) and crystallization enthalpy (ΔH_C) are 12.42 °C and 121.8 J/g, respectively. The phase transition temperatures and latent heats of the other composite phase change films are presented in Tables 4 and 5. It is worth mentioning that the addition of PLA as an encapsulation layer results in a noticeable reduction in the heat enthalpy of the PEG/PLA film compared to pure PEG. This is attributed to the fact that the PLA encapsulation matrix reduces the effective PEG content. As BN and OH-GN are incorporated, the latent heat of the composite films shows a gradual decrease. It is observed that the sample PCF-6 has the lowest enthalpy in all PEG/PLA/BN samples while PCF-11 presents the highest enthalpy amongst all PLA/PEG/OH-GN samples. Specifically, when 20% BN is added (sample PCF-6), the PEG/PLA/BN sample has a melting temperature of 37.03 °C, and a melting latent heat of 97.95 J/g. In a discharging process, the PCF-6 shows a freezing temperature of 18.46 °C and freezing latent heat of 89.48 J/g. The observed reduction in latent heat with the incorporation of 20 wt% boron nitride (BN) in the PEG/PLA composite phase change material (PCF-6) is primarily attributed to the volumetric dilution of the active PEG component. As BN is a thermally conductive but non-enthalpic filler, its presence reduces the relative mass fraction of PEG, thereby

decreasing the total amount of material available for solid/liquid phase transitions.

When 9% OH-GN is introduced (sample PCF-11), the melting temperature of PEG/PLA/OH-GN is 40.77 °C, with a melting latent heat of 136.5 J/g. The freezing temperature and freezing latent heat are 15.87 °C and 127.6 J/g, respectively. Comparatively, increasing the content of hydroxylated graphene (OH-GN) enhances the latent heat of the composite (samples PCF-7~PCF-11). This is because the abundant hydroxyl functional groups of OH-GN promotes strong hydrogen bonding and interfacial compatibility with PEG. The two-dimensional structured OH-GN groups provide high surface areas and serve as effective heterogeneous nucleation agents, which contribute to ordered PEG chain arrangement and stable phase transition domains. As a result, higher OH-GN content leads to an increased amount of energy stored and released during phase transitions, thereby raising the latent heat. This highlights the functional role of OH-GN in enhancing the thermal performance of PCFs in contrast to BN. Despite PCF-11 shows a maximum enthalpy amongst the PEG/PLA/OH-GN samples (PCF-7~ PCF-11), it still has a lower latent heat in charging/ discharging processes compared to the pure PEG. This can be explained by the volumetric dilution effect as aforementioned.

From Table 4 and Table 5, it is observed that the PEG/PLA/BN and PEG/PLA/OH-GN films show approximate melting temperatures and freezing temperatures to those of pure PEG. This indicates that the incorporation of BN and OH-GN does not significantly disrupt the intrinsic thermal transition behavior of the PEG phase. This suggests that the phase change mechanism of PEG remains largely preserved within the composite matrix. The maintained phase transition temperatures imply good thermal compatibility between PEG and the supporting PLA matrix, as well as with the BN and OH-GN fillers. The result also indicates that the physical confinement and interfacial interactions in the composite PCFs are not so restrictive as to hinder the thermal responsiveness of PEG, which is critical for ensuring a reliable and consistent energy storage system based on composite PCFs.

Although the observed freezing peak temperature is relatively low, it remains

well below the typical operational temperature range of electronic devices, thereby enabling the PCFs to undergo efficient heat absorption and release within the device's functional thermal window. This ensures efficient thermal management under diverse conditions. The high latent heat of the composite PCFs significantly enhances thermal energy storage capacity and contributes to reducing phase change hysteresis associated with supercooling effects, thus improving thermal responsiveness and efficiency of the PCF based systems. Moreover, the PCFs demonstrate excellent thermal cycling stability, exhibiting minimal degradation in phase change enthalpy after repeated melting/solidification cycles. This thermal durability reinforces its functional reliability over prolonged use, making it a promising candidate for advanced thermal management applications in electronics, where sustained performance, thermal buffering, and long-term stability are critical.

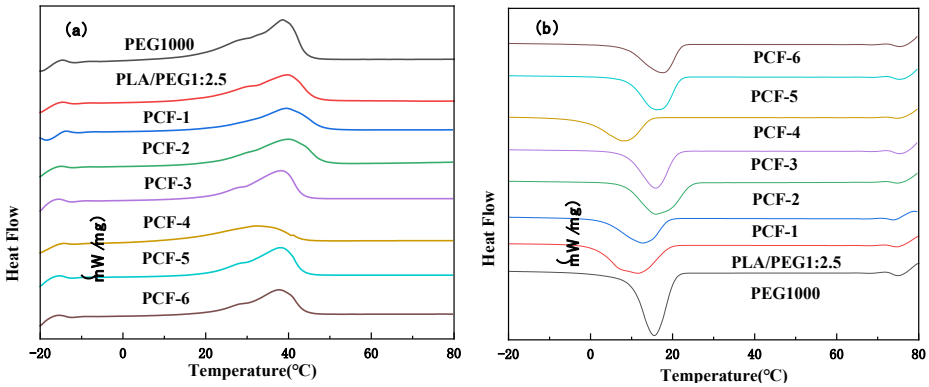

Figure 5 (a) melting curves of PEG 1000, PEG/PLA and PEG/PLA/BN; (b) Solidification curves of PEG 1000, PEG/PLA and PEG/PLA/BN

Table 4. Phase transition temperature and latent heat of PLA/PEG/BN phase transition films.

Samples	T_m (℃)	ΔH_m （J/g）	T_C (℃)	ΔH_C （J/g）
PEG1000	37.58	174.8	17.51	167.1
PLA/PEG1:2.5	39	124.7	12.42	121.8
PCF-1	38.97	118.3	13.53	121.2
PCF-2	40.46	113.1	16.85	120.9
PCF-3	38.89	110.9	16.98	103.8
PCF-4	31.87	109.7	8.6	103.7
PCF-5	37.41	107.9	17.42	102.8
PCF-6	37.03	97.95	18.46	89.48

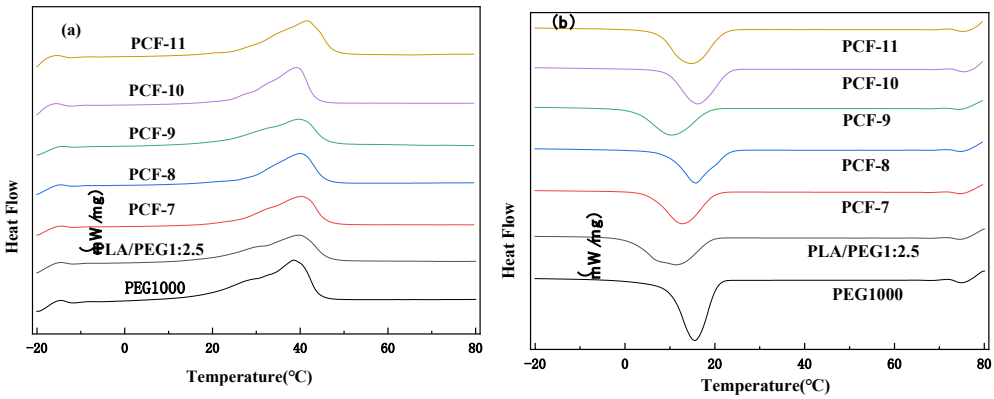

Figure 6 (a) melting curves of PEG 1000, PEG/PLA and PEG/PLA/OH-GN; (b) Solidification curves of PEG 1000, PEG/PLA and PEG/PLA/OH-GN

Table 5. Phase transition temperature and latent heat of PLA/PEG/OH-GN phase transition films.

Samples	T_m (℃)	ΔH_m（J/g）	T_C (℃)	ΔH_C（J/g）
PEG1000	37.58	174.8	17.51	167.1
PLA/PEG1:2.5	39.00	124.7	12.42	121.8
PCF-7	39.55	114.7	13.94	105.5
PCF-8	39.28	113.4	16.79	107.6
PCF-9	39.04	112.5	11.18	103.3
PCF-10	38.30	107.9	17.31	107.6
PCF-11	40.77	136.5	15.87	127.6

4.2 Thermal conductivity improvement

In practical applications, the thermal conductivity of composite films is a critical factor. Low thermal conductivity is one of the main drawbacks of polymers. In this study, the thermal conductivity of flexible phase change films was improved by incorporating different amounts of BN and OH-GN. Figure 7 illustrates the thermal conductivity of the films with various mass fractions of BN and OH-GN. The pure PLA/PEG film has a low thermal conductivity of only 0.18 W/(m·K), mainly due to the disordered polymer chains, which significantly impede phonon conduction. With the addition of high thermal conductivity fillers, the thermal conductivity of the phase change films was significantly improved. As shown in Figure 7(a), when 3% BN was added, the thermal conductivity of PCF-1 increased slightly to 0.19 W/(m·K). However, with the addition of 20% BN, the thermal conductivity of PCF-6 was signifi-

cantly enhanced to 0.4 W/(m·K). Generally, BN without a 3D network structure lacks sufficient thermal conductivity to effectively promote heat transfer within PLA/PEG films. In contrast, as shown in Figure 7(b), when 5% OH-GN is added, the thermal conductivity of PCF-9 increases to 0.41 W/(m·K) due to the higher thermal conductivity of OH-GN. Notably, the phase-change film with 9% OH-GN exhibits an outstanding thermal conductivity of 0.86 W/(m·K), which is 477.78% higher than that of the pure PLA/PEG film. The exceptionally small error bars in Fig. 7a and Fig. 7b indicate high measurement precision and reproducibility of the experiments, suggesting reliable experimental results based on the robust experimental methodology in various conditions.

The high thermal conductivity of the composite films can be attributed to the random distribution of OH-GN within the PLA matrix, which effectively mitigates phonon mismatch and promotes phonon transport at the interfaces. The thermal transport mechanism of this material relies on the synergistic effect between a three-dimensional thermal conduction network and phase-change regulation: the oxidized graphene/boron nitride composite establishes continuous heat transfer pathways to enable rapid thermal conduction, while the phase-change matrix dynamically regulates heat flow through solid-liquid phase transitions, endowing the system with both efficient heat transfer and controllable heat release characteristics. Therefore, the addition of BN and OH-GN further optimizes the thermal conductivity of the flexible phase-change films. Based on the thermal conductivity measurements, the heat transfer rate of the samples was analyzed using the time-temperature (t-T) curve, as shown in Figure 7(c). Samples with the same thickness (approximately 0.5 mm), including PCF-11, PCF-6, and the control sample, were placed on a heating platform and heated to 70 °C, with temperature changes monitored by thermocouples. The results indicate that PCF-11 exhibited a higher heating rate compared to both PCF-6 and the PLA/PEG sample. When reaching the same temperature (50 °C), the times required were 191.49 seconds, 194.26 seconds, and 203.36 seconds, respectively. At 191.49 seconds, the temperatures of the PCF-11 and PCF-6 films were 2.7 °C and 1.7 °C

higher than that of the control sample, respectively. The faster temperature rise observed in PCF-11 indicates its superior thermal conductivity, which is consistent with the thermal conductivity data. This further confirms that the incorporation of OH-GN significantly enhances the heat transfer performance of the composite films. The composite films were placed on a heating plate, and the temperature distribution during the heating process was measured. Real-time temperature variations were recorded using an infrared thermal imaging camera. Figures 7(d-i) illustrate the temperature changes of the samples. As seen, compared to PLA/PEG and PCF-6, the PCF-11 sample demonstrates a faster heating rate and superior thermal diffusion capacity. This result underscores the outstanding heat dissipation performance of the PCF-11 composite film, making it highly suitable for thermal management of electronic devices.

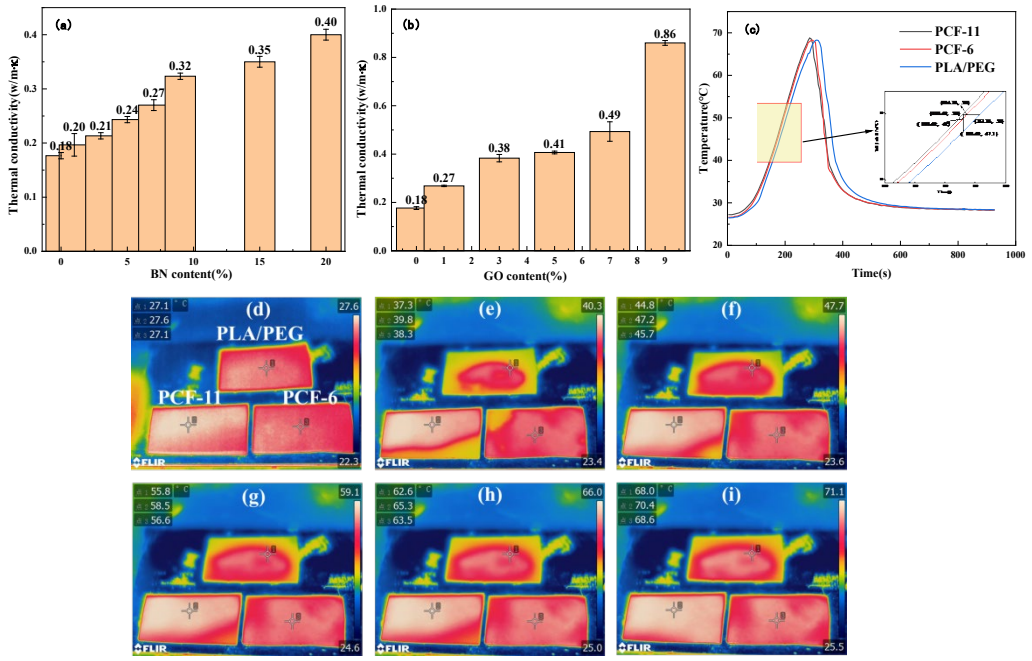

Figure 7 (a) Variation of thermal conductivity of phase change thin films with BN content; (b) The thermal conductivity of the phase change film varies with the OH-GN content; (c) t-T curves of PLA/PEG, PCF-6 and PCF-11; (d-i) Photos of sample heating process and infrared thermal imaging pictures.

4.3 Thermal stability analysis

The thermal stability of phase change films is a critical factor for their practical applications. The melting and crystallization curves, as well as the enthalpy values of

559 the PCF-6 and PCF-11 films after 10, 30, and 50 thermal cycles, are presented in Fig-
560 ure 8 (a-c). From the figure, it can be observed that after 50 thermal cycles, the en-
561 thalpy values of the PCF-6 and PCF-11 films decrease by 3.4% and 3.22%, respec-
562 tively.

563 To ensure the reliability and reproducibility of the thermal stability analysis, strict
564 adherence to sample mass uniformity was maintained throughout all cyclic experi-
565 ments. In the experiments, each DSC sample was precisely weighed to approximately
566 10 mg, with a tolerance of ±0.5 mg, prior to encapsulation in liquid aluminum cruci-
567 bles. This mass control was critical for minimizing variability in thermal performance
568 of the PCFs attributable to possible inconsistency of sample mass differences. The
569 encapsulated samples were subsequently subjected to thermal cycling within a con-
570 trolled environmental chamber, which allowed for precise regulation of temperature
571 and atmosphere during the entire testing sequence. Furthermore, the use of sealed
572 aluminum crucibles effectively prevented any potential mass loss caused by sample
573 volatilization or decomposition during thermal cycling. This containment strategy
574 ensured that the sample mass remained constant over multiple charging/ discharging
575 cycles, thereby eliminating mass change as a confounding factor in the DSC results.

576 As a result, the experimental results obtained reflect intrinsic properties and gen-
577 uine thermal stability of the fabricated PCFs, rather than artifacts arising from sample
578 degradation or measurement inconsistencies. Therefore, it can be concluded that the
579 prepared phase change films demonstrate an excellent thermal stability under diverse
580 heat flow conditions. The above mass control protocol underpins the validity of the
581 cyclic DSC measurements and superior cyclic stability of the PCFs samples.

582 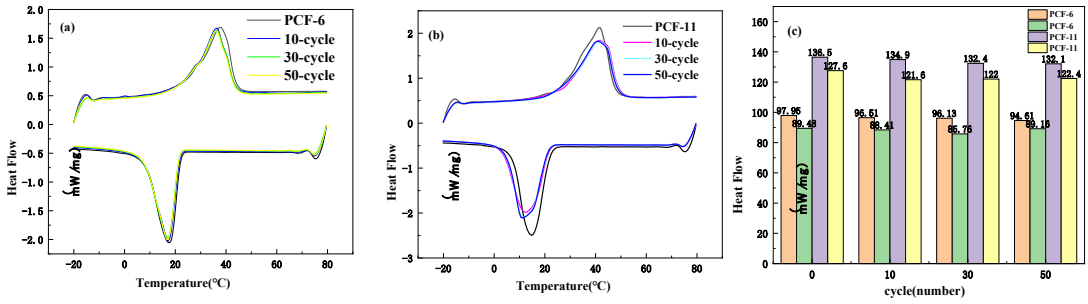

Figure 8 (a) Melting and crystallization curves of PCF-6 film before and after 10, 30 and 50 cycles; (b) Melting and crystallization curves of PCF-11 film before and after 10, 30 and 50 cycles; (c) Melting enthalpy and crystallization enthalpy of PCF-6 and PCF-11 films before and after 10, 30 and 50 cycles.

5 Application of composite PCFs for electronics cooling

Based on the results of leakage prevention, phase change behavior, thermal stability, and thermal conductivity analysis, the PCF-11 film was chosen for thermal management testing. To further assess the thermal energy storage and release characteristics of the PCF-11 film, both PCF-11 and the control sample (PLA film) were placed on a heating plate and heated from room temperature to 75 °C. During this process, an infrared camera was used to capture the transient temperature response of both the PCF-11 and control samples, allowing for a detailed evaluation of their heat storage performance. The temperature distribution of PCF-11 and the control sample is shown in Figure 9 (a-f). During the initial heating phase, PCF-11 displays a significantly lower temperature compared to the control sample, highlighting its exceptional latent heat storage capacity. As heating continues, both PCF-11 and the control sample gradually shift from latent heat storage to sensible heat storage, leading to a noticeable rise in temperature for both materials. To investigate the thermal energy release process of the phase-change film, PCF-11 and the control sample were first heated on a 60 °C heating platform for a period of time. Afterward, the samples were removed from the heating plate and allowed to cool naturally at room temperature. The transient temperature changes were recorded using an infrared camera, as shown in Figures 9(g-l). Due to the excellent latent heat release properties of PCF-11, its temperature during the cooling process remained significantly higher than that of the control sample, demonstrating its effective insulation capability. This indicates that the PCF film possesses excellent phase-change cooling functionality, offering great potential for future thermal management applications.

The composite phase-change film effectively integrates thermal energy storage, heat transfer, and light absorption, demonstrating great potential for applications in

solar thermal utilization. To investigate the photothermal conversion performance of the composite phase-change films, a solar simulation system was set up, as shown in Figure 9(m). The system consists of three components: a solar simulator, a temperature measurement device, and a computer. The simulated solar intensity was set to 144 mW/cm^2. The PCF-11 film and the control sample (PLA/PEG) were placed on glass dishes, and thermocouples were fixed using insulating tape and cotton for insulation and testing. Meanwhile, a computer was used to capture the transient temperature distribution and record the temperature changes of the phase-change films. After the phase-change process of the composite films was completed, the simulated solar light source was turned off, and the samples were left to cool naturally. Figure 9(n) shows the temperature variation under simulated solar irradiation. As the sample is exposed to light, the temperature approaches the phase transition point, causing the temperature to increase slowly and creating a plateau. This indicates that the composite phase change film undergoes a phase transition under simulated solar irradiation, where solar energy is converted into heat and stored in the phase change material. Under a light intensity of 144 mW/cm^2, the PCF-11 film completes its solid-liquid phase transition in 205 seconds. After the phase transition, the temperature rises rapidly. At 212 seconds of exposure to the same solar radiation, the surface temperature of the PCF-11 composite film reaches 50 °C, which is 14.14 °C higher than that of the PLA/PEG film. This enhanced performance is attributed to the superior light absorption and high photothermal conversion capabilities of the graphene-based PCF-11 film, enabling it to efficiently absorb solar energy and convert it into heat. When the light source is turned off and the sample is allowed to cool naturally, the temperature decreases rapidly, following a trend that aligns with the heat release curve shown in Figure 7(c). These results demonstrate that graphene exhibits strong light absorption characteristics, highlighting its great potential for solar thermal utilization. The photothermal conversion efficiency (λ) of the composite film can be calculated using the following formula:

$$\lambda = \frac{m\Delta Hm}{PA\Delta t} \times 100\% \quad (1)$$

Where m, ΔHm, Δt, and A represent the weight (g), melting enthalpy (J/g), melting phase transition time (s), and surface area (cm^2) of the composite film, respectively. P is the light power density of the simulated sunlight (mW/cm^2). The light power density of the simulated sunlight P is measured in mW/cm^2. The photothermal conversion efficiency of the PCF-11 composite film reaches 91.7%, enabling the PCF-11 film to rapidly absorb solar energy and convert it into thermal energy, effectively achieving thermal insulation. The photothermal conversion mechanism of PCFs primarily relies on the unique structure and properties of oxidized graphene. The two-dimensional structure and abundant oxygen-containing functional groups on the surface of oxidized graphene endow it with excellent broadband light absorption capabilities, enabling effective capture of solar energy. These functional groups facilitate the conversion of light energy into thermal energy. Furthermore, the strong interfacial bonding between oxidized graphene and the phase-change matrix material ensures efficient storage and utilization of the converted thermal energy. These results highlight the high photothermal conversion efficiency of graphene and its crucial role in the photothermal conversion process.

To assess the thermal management performance of the PCF film, both PLA and PCF-11 films were placed on a constant temperature heating plate to simulate heat generation in electronic devices. The surface temperature of the films was recorded using an infrared thermal imaging camera. The test results are shown in Figures 9(o-t), where the heating plate is maintained at a temperature of 47 °C. Upon contacting the heating plate, the PLA film was quickly heated up to 44 °C. In contrast, the temperature of the PCF-11 film gradually increased from 38 °C to 43.5 °C within 150 seconds. This temperature difference can be attributed to the solid-liquid phase change behavior of polyethylene glycol. This demonstrates that when the PCF-11 film is applied to heat-generating devices, it can effectively conduct and absorb the accumulated heat, helping to mitigate the rapid temperature rise in electronic devices. The experimental

results, obtained by simulating heat generation in electronic devices using a constant temperature heating plate and recording the surface temperature of the film, demonstrate that the PCF-11 material exhibits outstanding buffering effects during thermal management. Compared to conventional materials, this composite film significantly delays the temperature rise and promotes more uniform heat distribution, attributed to the solid-liquid phase change behavior of polyethylene glycol. Although supercooling occurs, the combined effects of high latent heat and thermal conductive fillers ensure effective thermal management, suggesting that the impact of supercooling on thermal performance is minimal.

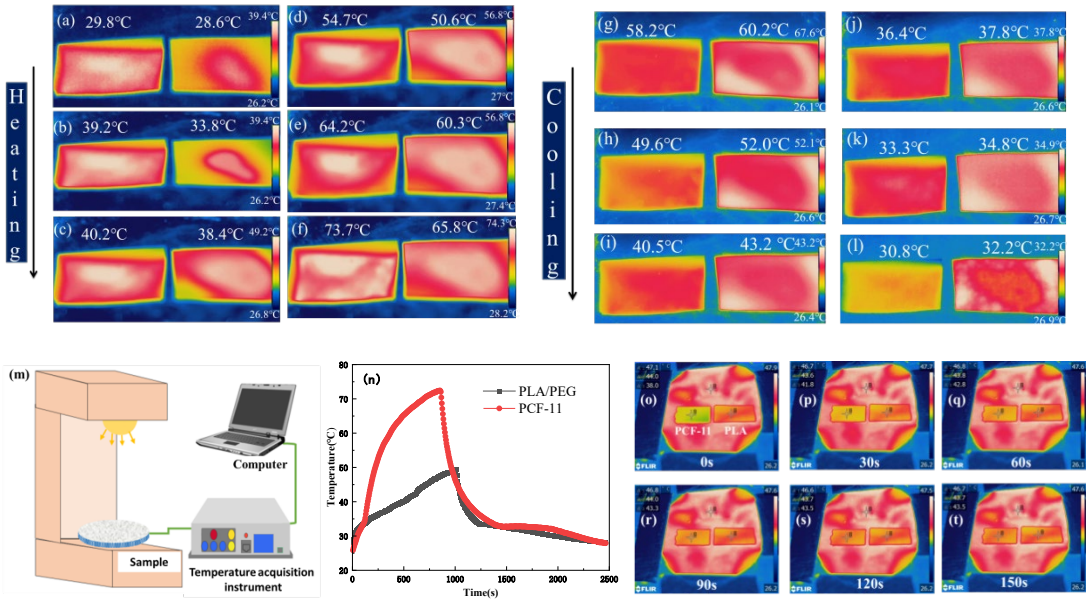

Figure 9 (a-f) FTIR images of PLA (left) and PCF-11 (right) during thermal energy storage of the heating plate; (g-l) FTIR images of PLA and PCF-11 during thermal energy release; (m) Photothermal conversion test experimental system; (n) Temperature curves of PLA/PEG and PCF-11 photo thermal conversion; (o-t) Temperature control infrared image of PLA and PCF-11 films on constant temperature heating plate in 150s.

This study systematically evaluated the functional performance of the composite PCFs (i.e. PCF-11), demonstrating its exceptional potential for advanced thermal management applications. Through detailed experimental analyses, PCF-11 was shown to possess a highly effective phase change temperature regulation mechanism

that enables intelligent bidirectional thermal control. During the heating phase, the film maintains significantly lower surface temperatures than conventional PLA films, while in the cooling phase, it sustains elevated temperatures for longer durations. This behavior is attributed to the composite's optimized latent heat storage and release capability, which ensures thermal inertia and reduces temperature fluctuations. The incorporation of polyethylene glycol (PEG) within a flexible PLA matrix provides a stable and reversible thermal transition environment, enhancing both performance consistency and mechanical durability. These features enable the film to adapt effectively to varying temperature profiles, making it suitable for dynamic thermal environments such as wearable electronics or solar heat collection systems. The enhanced flexibility and surface conformability further improve the integration potential of PCFs into irregular surfaces or layered system architectures.

In addition to phase change performance, the composite PCFs (i.e. PCF-11) demonstrate superior photothermal conversion and thermal buffering capabilities, further enhancing its application value. By incorporating graphene as a thermally conductive and optically absorptive filler, the photothermal conversion efficiency of the film is significantly increased to 91.7%. Under simulated solar irradiation of 144 mW/cm^2, the PCF-11 film completes its full phase transition in 205 seconds, outperforming the PLA/PEG control by achieving a surface temperature that is 14.14 °C higher. This efficiency highlights its strong solar energy harvesting and conversion potential, positioning it as an ideal candidate for solar thermal collector systems. Furthermore, in simulated electronic heat dissipation scenarios, PCF-11 exhibits a pronounced temperature buffering effect. It delays the temperature rise of underlying components by 150 seconds and maintains a more stable thermal profile, as evidenced by less fluctuating temperature curves. This thermal dampening capacity is critical for protecting temperature-sensitive electronics from rapid thermal spikes, improving both performance reliability and operational lifespan. The synergy of the high latent heat, graphene-enhanced heat conduction and flexible structure adaptability of the PCFs provides a comprehensive thermal management solution suited for high-power

electronics, smart textiles and next-generation energy storage systems.

6. Concluding remarks

In this study, BN/OH-GN based composite phase change films (PCFs) were fabricated using a solution blending method, offering a practical and scalable approach for the development of high-performance thermal management materials. By constructing an interconnected three-dimensional thermally conductive network within the PLA/PEG matrix, the composite films successfully addressed several critical scientific and engineering challenges commonly faced by conventional phase change materials (PCMs). These include inherently poor mechanical properties, leakage at elevated temperatures, and thermal degradation after repeated cycling.

The results demonstrate a significant improvement in mechanical performance, with the elongation at break increased by 32.5 times compared to pure PLA, indicating excellent flexibility and durability of the PCFs. In addition, the films maintained structural integrity at 80 °C, confirming their superior shape stability and leakage resistance under practical thermal conditions. Importantly, the composite PCFs retained a high phase change enthalpy (up to 136.5 J/g), ensuring efficient thermal energy storage, while exhibiting exceptional thermal cycling stability with less than 3.5% enthalpy loss after 50 cycles. The integration of BN and OH-GN also led to a marked enhancement in thermal conductivity of 0.86 W/(m·K), and a high photothermal conversion efficiency of 91.7%, which is largely attributed to the synergistic effects of the conductive fillers and graphene's light-absorbing properties.

This study provides valuable insights into the rational design of flexible and high-performance composite PCMs, enabling the applicability of PCFs in demanding environments due to their superior thermal energy storage and regulation capabilities. The fabricated PCFs are integral to solar thermal collector systems, enhancing heat capture and retention efficiency. In advanced textile engineering, composite PCMs provide effective thermal insulation, improving comfort and energy conservation. Their incorporation into intelligent thermal management systems enables dynamic temperature regulation in electronic devices and building environments. Furthermore,

746 composite PCMs play a crucial role in wearable electronics by maintaining thermal
747 stability and user comfort during operation. Overall, these materials offer promising
748 solutions for sustainable energy storage and temperature control technologies.

749 **Acknowledgements**

750 The work was supported by the Central Plains Science and Technology Innovation
751 Leading Talents Project of Henan Province (234200510011), the Henan Key Research
752 and Development Program (241111320900, 231111320900), Key Technologies R&D
753 Program of Henan Province (232102241018）and the guiding fund of government's
754 science and technology (Z20241471018).

755 **References**

756 [1] A. Farzanehnia, M. Khatibi, M. Sardarabadi, M. Passandideh-Fard, Experimental
757 investigation of multiwall carbon nanotube/paraffin based heat sink for electronic
758 device thermal management, Energy Convers. Manage. 179 (2019) 314-325.
759 [2] H.X. Zeng, J.Y. Wu, H.J. Pei, Y.K. Zhang, Y.S. Ye, Y.G. Liao, X.L. Xie, Highly
760 thermally conductive yet mechanically robust composites with nacre-mimetic
761 structure prepared by evaporation-induced self-assembly approach, Chem. Eng. J.
762 405 (2021) 126865.
763 [3] L.Y. Yang, C.P. Feng, L. Bai, R.Y. Bao, Z.Y. Liu, M.B. Yang, W. Yang, Flexible
764 shape-stabilized phase change materials with passive radiative cooling capability
765 for thermal management, Chem. Eng. J. 425 (2021) 131466.
766 [4] G. Hekimoğlu, M. Nas, M. Ouikhalfan, A. Sarı, Ş. Kurbetci, V.V. Tyagi, R.K.
767 Sharma, T.A. Saleh, Thermal management performance and mechanical
768 properties of a novel cementitious composite containing fly ash/lauric
769 acid-myristic acid as form-stable phase change material, Constr. Build. Mater.
770 274 (2021) 122105.
771 [5] Y. Kou, K.Y. Sun, J.P. Luo, F. Zhou, H.B. Huang, Z.S. Wu, Q. Shi, An intrinsically
772 flexible phase change film for wearable thermal managements, Energy. Storage.
773 Mater 34 (2021) 508-514.
774 [6] S.P. Chitriv, K. Dharmadhikari, A. Nithin, A.S. Archak, R.P. Vijayakumar, G.C.
775 Dsouza, Unzipped multiwalled carbon nanotube oxide / PEG based phase change
776 composite for latent heat energy storage, Int. J. Heat Mass Transfer 220 (2024)
777 124908.
778 [7] H.D. Pang, G.H. Li, L.Q. Cheng, C. He, X.M. Wang, X. Zhang, 3D flower-like
779 CuO@PEG composite phase change materials with photo response for
780 applications in energy conversion and storage, Journal of Energy Storage 82
781 (2024) 110537.
782 [8] X.D. Cheng, Q.G. Feng, W.L. Ni, X. Li, Y. Qi, S.Y. Zhang, Q.H. Wu, Z.Y. Huang,
783 Stable and reliable PEG/TiO_2 phase change composite with enhanced thermal

conductivity based on a facile sol-gel method without deionized water, J. Energy. Storage 89 (2024) 111705.
[9] X. Lu, H.W. Huang, X.Y. Zhang, P.C. Lin, J.T. Huang, X.X. Sheng, L. Zhang, J.P. Qu, Novel light-driven and electro-driven polyethylene glycol/two-dimensional MXene form-stable phase change material with enhanced thermal conductivity and electrical conductivity for thermal energy storage, Compos. Part B-Eng 177 (2019) 107372.
[10] P. Cheng, X. Chen, H.Y. Gao, X.W. Zhang, Z.D. Tang, A. Li, G. Wang, Different dimensional nanoadditives for thermal conductivity enhancement of phase change materials: Fundamentals and applications, Nano Energy 85 (2021) 105948.
[11] Y.P. Xia, H.Z. Zhang, P.R. Huang, C.W. Huang, F. Xu, Y.J. Zou, H.L. Chu, E. Yan, L.X. Sun, Graphene-oxide-induced lamellar structures used to fabricate novel composite solid-solid phase change materials for thermal energy storage, Chem. Eng. J. 362 (2019) 909-920.
[12] W.Q. Du, H. Fei, Y.C. Pan, Q. He, J.H. Zhou, X.M. Liang, Development of capric acid-stearic acid-palmitic acid low-eutectic phase change material with expanded graphite for thermal energy storage, Constr. Build. Mater. 320 (2022) 126309.
[13] H.Y. Wu, S.T. Li, Y.W. Shao, X.Z. Jin, X.D. Qi, J.H. Yang, Z.W. Zhou, Y. Wang, Melamine foam/reduced graphene oxide supported form-stable phase change materials with simultaneous shape memory property and light-to-thermal energy storage capability, Chem. Eng. J. 379 (2020) 122373.
[14] H.L. Hu, Recent advances of polymeric phase change composites for flexible electronics and thermal energy storage system, Compos. Part B-Eng 195 (2020) 108094.
[15] Y. Liang, H.B. Yang, H.D. Tang, J.Y. Chen, Y.C. Wang, H.Z. Cui, Influence of metal encapsulation on thermophysical properties and heat transfer in salt hydrate phase change material for air conditioning system, Sustain.Energy Technol.Assess. 62 (2024) 103618.
[16] M. Zhou, T.Q. Lin, F.Q. Huang, Y.J. Zhong, Z. Wang, Y.F. Tang, H. Bi, D.Y. Wan, J.H. Lin, Highly Conductive Porous Graphene/Ceramic Composites for Heat Transfer and Thermal Energy Storage, Adv. Funct. Mater. 23(18) (2012) 2263-2269.
[17] J.M. Shi, M.L. Qin, W. Aftab, R.Q. Zou, Flexible phase change materials for thermal energy storage, Energy. Storage. Mater 41 (2021) 321-342.
[18] C.X. Deng, H.S. Dong, Y. Kou, H.Q. Liu, K.Y. Sun, W.W. Jian, Q. Shi, Flexible self-healing phase change film with high transition enthalpy for thermal management, J. Energy. Storage 62 (2023) 106873.
[19] Q.H. Ji, X.X. Sheng, X.L. Li, S. Liu, Q.F. Chen, P.Z. Guo, Y.B. Yang, Y.Y. Huang, G.L. Zhang, X. Lu, J.P. Qu, Camel skin-fat structure inspired MXene@PVA/PCC aerogel composite for efficient medium and low temperature infrared stealth, Chemical Engineering Journal 476 (2023) 146671.
[20] H. Fang, J.M. Zeng, X.Y. Shao, D.Y. Hu, Advanced electromagnetic shielding

and excellent thermal management of flexible phase change composite films, Carbon 215 (2023) 118442.
[21] K. Sun, H.S. Dong, Y. Kou, H.N. Yang, H.Q. Liu, Y.G. Li, Q. Shi, Flexible graphene aerogel-based phase change film for solar-thermal energy conversion and storage in personal thermal management applications, Chem. Eng. J. 419 (2021) 129637.
[22] H. Liu, L.Y. Li, X.X. Tian, X.D. Wang, Flexible phase-change composite films for infrared thermal camouflage and photothermal energy storage, J. Energy. Storage 73 (2023) 109203.
[23] Z.K. Bai, Z.Y. Yao, G.M. Wu, K.W. Liu, D.Z. Ye, Y.Z. Tao, S.L. Xiao, D.Z. Chen, Z.M. Deng, J. Xu, Y.S. Zhou, S.J. Wei, X.Z. Yin, PU/PVDF blend nanofiber film with enhanced mechanical and piezoelectric performance for development of stable nanogenerators, Sens. Actuators. A. Phys. 357 (2023) 114407.
[24] X. Huang, G. Alva, L.K. Liu, G.Y. Fang, Microstructure and thermal properties of cetyl alcohol/high density polyethylene composite phase change materials with carbon fiber as shape-stabilized thermal storage materials, Appl. Energy 200 (2017) 19-27.
[25] K. Xu, X.H. Xu, T. Yan, Performance evaluation of a pipe-embedded phase change material (PE-PCM) roof integrated with solar collector, Journal of Building Engineering 71 (2023) 106582.
[26] K. Zhao, J.F. Wang, H.Q. Xie, A multifunctional flexible composite phase-change film with excellent solar driven thermal management, Renew. Energy. 227 (2024) 120534.
[27] X.Y. Zhang, K.Y. Sun, H.Q. Liu, J. Chen, X.M. Yan, Y. Kou, Q. Shi, Flexible insulating phase change composite film with improved thermal conductivity for wearable thermal management, Nano Energy 121 (2024) 109256.
[28] W. Aftab, A. Mahmood, W. Guo, M. Yousaf, H. Tabassum, X. Huang, Z. Liang, A. Cao, R. Zou, Polyurethane-based flexible and conductive phase change composites for energy conversion and storage, Energy. Storage. Mater 20 (2019) 401-409.
[29] Y.J. Tang, Y.X. Lin, Y.T. Jia, G.Y. Fang, Improved thermal properties of stearyl alcohol/high density polyethylene/expanded graphite composite phase change materials for building thermal energy storage, Energy. Build. 153 (2017) 41-49.
[30] X. Geng, Y.Y. Hu, H. Pan, C.Y. Wang, Z.M. Liu, X. He, Biodegradable polylactic acid/polyethylene glycol blends as form-stable phase change materials for thermal energy storage and management, Polymer 300 (2024) 127023.
[31] S.C. Zhang, P.Q. Liu, Y. Chen, C. Campagne, F. Salaün, Electrospraying poly(lactic acid) microcapsules loaded with n-hexadecane for thermal energy storage systems, Mater. Today. Commun. 33 (2022) 104443.
[32] X.M. Yang, M.H. Zhou, P.R. Arévalo, L.S. Mesa, G.Z. Yin, Chitosan incorporation for improving the dimensional stability of PLA aerogel encapsulated phase change materials, Mater. Lett. 351 (2023) 135050.
[33] M.J. Sheng, Y.J. Sheng, H. Wu, Z.G. Liu, Y. Li, Y. Xiao, X. Lu, J.P. Qu, Bio-based poly (lactic acid) shaped wood-plastic phase change composites for

thermal energy storage featuring favorable reprocessability and mechanical properties, Sol. Energy Mater. Sol. Cells 252 (2023) 135050.
[34] R. Kumar, Y. Alex, B. Nayak, S. Mohanty, Effect of poly (ethylene glycol) on 3D printed PLA/PEG blend: A study of physical, mechanical characterization and printability assessment, J. Mech. Behav. Biomed. Mater. 141 (2023) 105813.
[35] B. Wang, K. Hina, H.T. Zou, D.Y. Zuo, C.H. Yi, Thermal, crystallization, mechanical and decomposition properties of poly(lactic acid) plasticized with poly(ethylene glycol), J. Vinyl. Addit. Technol. 24 (2018) 154-163.
[36] Z.C. Chen, M. Xu, C. Zhou, Z.Y. Hu, Z.L. Du, X.M. Fu, Y.H. Song, Y.B. Jia, X.J. Wen, J.F. Wang, G.M. Cai, S.W. Yang, X.Z. Yin, Phase transformation enabled textile triboelectric nanogenerators for wearable energy harvesting and personal thermoregulation, Nano Energy 132 (2024) 110361.
[37] L.Y. Jing, Y.H. Song, S.Y. He, X.M. Fu, Z.L. Du, X.Z. Yin, Dual-mode driven Marangoni actuator with spontaneity and controllability as a soft robot, Sensors and Actuators B-Chemical 436 (2025) 137697.
[38] R.R. Cao, S. Chen, Y.Z. Wang, N. Han, H.H. Liu, X.X. Zhang, Functionalized carbon nanotubes as phase change materials with enhanced thermal, electrical conductivity, light-to-thermal, and electro-to-thermal performances, Carbon 149 (2019) 263-272.
[39] D. Hu, L. Han, W.Q. Zhou, P. Li, Y. Huang, Z. Yang, X.L. Jia, Flexible phase change composite based on loading paraffin into cross-linked CNT/SBS network for thermal management and thermal storage, Chem. Eng. J. 437 (2022) 135056.
[40] Y.J. Tang, Y.T. Jia, G. Alva, X. Huang, G.Y. Fang, Synthesis, characterization and properties of palmitic acid/high density polyethylene/graphene nanoplatelets composites as form-stable phase change materials, Sol. Energy Mater. Sol. Cells 155 (2016) 421-429.
[41] J. Gao, B. Zhou, C.Q. Liu, C.E. He, Y.Z. Feng, C.T. Liu, Carbonization welding graphene architecture for thermally conductive phase change composites with solar/electric-to-heat conversion ability, Chemical Engineering Journal 475 (2023) 146087.
[42] Y.Q. Guo, Z.Y. Lyu, X.T. Yang, Y.J. Lu, K.P. Ruan, Y.L. Wu, J. Kong, J.W. Gu, Enhanced thermal conductivities and decreased thermal resistances of functionalized boron nitride/polyimide composites, Compos. Part B-Eng 164 (2019) 732-739.
[43] T. Huang, T. Wang, J. Jin, M. Chen, L.M. Wu, Design of Silicon Rubber/BN Film with High Through-plane Thermal Conductivity and Ultra-low Contact Resistance, Chemical Engineering Journal 469 (2023) 143874.
[44] D.F. Gan, Q. Huang, J.J. Dou, H.Y. Huang, J.Y. Chen, M.Y. Liu, Y.Q. Wen, Z.Y. Yang, X.Y. Zhang, Y. Wei, Bioinspired functionalization of MXenes ($Ti_3C_2T_X$) with amino acids for efficient removal of heavy metal ions, Appl. Surf. Sci. 504 (2020) 144603.
[45] Y. Mao, J. Li, X. Yang, K. Tao, K. Sun, S. Chen, Y. Zheng, Heat transfer properties of graphene/polyethylene glycol composite phase change material modified by bifunctional titanate coupling agent, J. Energy. Storage 116 (2025)

115803.
[46] Z. Zhou, H. Xia, J. Hu, L. Wang, Enhanced thermal energy storage of polyethylene glycol composite with high thermal conductive reaction-bonded BN aerogel, Composites Communications 49 (2024) 101965.